DOI: 10.1002/ ((please add manuscript number))

Article type: Full Paper

Effect of Dielectric Environment on Excitonic Dynamics in Monolayer WS2

Yang Fu, Dawei He, Jiaqi He, Ang Bian, Lu Zhang, Shuangyan Liu, Yongsheng Wang*,

and Hui Zhao*

Y. Fu, Prof. D. He, A. Bian, L. Zhang, S. Liu, Prof. Y. Wang

Key Laboratory of Luminescence and Optical Information, Ministry of Education,

Institute of Optoelectronic Technology, Beijing Jiaotong University, Beijing 100044,

China

E-mail: huizhao@ku.edu

yshwang@bjtu.edu.cn

Dr. J. He

College of Mathematics and Physics, Beijing University of Chemical Technology,

Beijing 100029, China

Prof. H. Zhao

Department of Physics and Astronomy, The University of Kansas, Lawrence, Kansas

66045, United States

Keywords: 2d materials, excitons transport, photocarriers, transient absorption

Abstract

We report an experimental study on the effect of hexagonal boron nitride (h-BN)

underlay and cap layers on excitonic dynamics in monolayer WS₂. A monolayer WS₂

flake was fabricated by mechanical exfoliation. By using a dry transfer technique, three

regions of the sample were obtained: WS2 directly on SiO2, WS2 on h-BN, and WS2

sandwiched by two h-BN flakes. Photoluminescence measurements show higher yield

and narrower linewidth of the h-BN/WS₂/h-BN region. Transient absorption

measurements revealed that the top h-BN layer enhances the exciton formation,

prolongs the exciton lifetime, and slightly affects the exciton-exciton annihilation. By

performing spatially resolved transient absorption measurements, we obtained exciton diffusion coefficients of about 100, 40, and 26 square centimeters per second for the regions of WS₂, h-BN/WS₂, and h-BN/WS₂/h-BN, respectively. The suppression of exciton diffusion by h-BN is attributed to the additional phonon scattering mechanisms introduced by h-BN, which decreases the exciton mean free path and thus the diffusion coefficient. Our findings provide useful information for designing and understanding the effect of h-BN layers interfacing with two-dimensional semiconductors.

1 Introduction

Since 2010, two-dimensional (2D) transition metal dichalcogenides (TMDs) have been extensively studied as new semiconducting materials. ^[1] They have shown elusive properties, such as large absorption coefficients, thickness-tunable bandgaps^[2-3] and novel optical properties, ^[4-8] which make them attractive candidates for next-generation and ultrathin optoelectronic devices, including solar cells, ^[9] photodetectors, ^[9] and light-emitting diodes. ^[10-12] One unique feature of 2D TMDs is their large exciton binding energies on the order of hundreds of meV, ^[13-16] which make excitons stable at elevated temperatures. Therefore, excitons play a key role in determining the optical and optoelectronic properties of 2D TMDs. Hence, understanding the dynamics of excitons in these materials is important for their applications.

Recently, various aspects of exciton dynamics in 2D TMDs have been studied, including thermalization and energy relaxation, [17] exciton formation, [18] exciton-exciton annihilation, [19-20] exciton diffusion, [21-23] spin and valley relaxation, [24-32] and

exciton recombination. ^[19, 24, 28, 33-40] Although these studies have provided a solid foundation to understand excitonic dynamics in 2D TMDs, one key issue has been less investigated, namely the effect of the dielectric environment experienced by the excitons. In most of these studies, the 2D TMD samples were on SiO₂ substrates and exposed to a vacuum or air. It has been generally recognized that the dielectric environment can be used to tune the optical and electronic properties of 2D materials by altering Coulomb interactions between charge carriers. ^[7, 13, 15-18, 41-45] For example, if a TMD monolayer (1L) is covered by a dielectric material, the introduced screening can alter its electronic and optical properties. ^[46-57] However, little was known on how do such dielectric layers affect the excitonic dynamics. Such knowledge is not only useful for designing certain dielectric structures to engineering dynamical properties of excitons in these materials; it is also necessary since in practical devices the 2D materials are often integrated with dielectric materials. For example, hexagonal boron nitride (*h*-BN) has been widely used as underlay or cap layers of 2D devices.

Here we report an experimental study on the effect of *h*-BN underlay and cap layers on excitonic dynamics in 1L WS₂. By spatially and temporally resolved transient absorption measurements, we studied exciton dynamics in three regions of a single 1L WS₂ flake with different types of dielectric environments: air/WS₂/SiO₂, air/WS₂/*h*-BN, and *h*-BN/WS₂/*h*-BN. We found that the top *h*-BN layer enhances the exciton formation, prolongs the exciton lifetime, and slightly affects the exciton-exciton annihilation. We obtained exciton diffusion coefficients of about 100, 40, and 26 cm² s⁻¹ in these three regions, respectively. The suppression of exciton diffusion by *h*-BN is attributed to the

additional phonon scattering mechanisms introduced by *h*-BN, which decreases the exciton mean free path and thus the diffusion coefficient. Our findings provide useful information for designing and understanding the effects of *h*-BN layers interfacing with 2D semiconductors.

2 Results and discussion

2.1 Steady-state characterization

Figure 1a shows the structure of the sample, which is composed of a WS₂ 1L with different dielectric environments: air/SiO₂, h-BN/SiO₂, and h-BN/h-BN. We note that it is important that all the three regions are achieved on a single WS₂ 1L flake, so that sample-to-sample variations can be largely eliminated. The sample was fabricated by a standard mechanical exfoliation and dry transfer technique.^[58] Figure 1b shows an optical microscope image of the sample. The top and bottom h-BN layers are 317 and 95 nm, respectively, which are determined by atomic force microscope measurements. Since both thicknesses are much larger than the range of the Coulomb field between electrons and holes of a few nanometers, each h-BN layer can screen the entire field that extends beyond WS₂. Hence, they can be considered as bulk h-BN. The specific values of the thickness are less significant and we do not expect the observed effects to be dependent on the thickness in this regime. The 1L thickness of the WS₂ flake was first inferred from the green-channel contrast of its microscope image when on PDMS and then confirmed by its Raman spectrum after transferred to Si/SiO2. As shown in Figure 1c, the position of the A_{1g} and E_{2g}^1 peaks in the Raman spectrum and their separation of 65 cm⁻¹ are consistent with previously reported values for 1L WS₂ on such substrates.^[59]

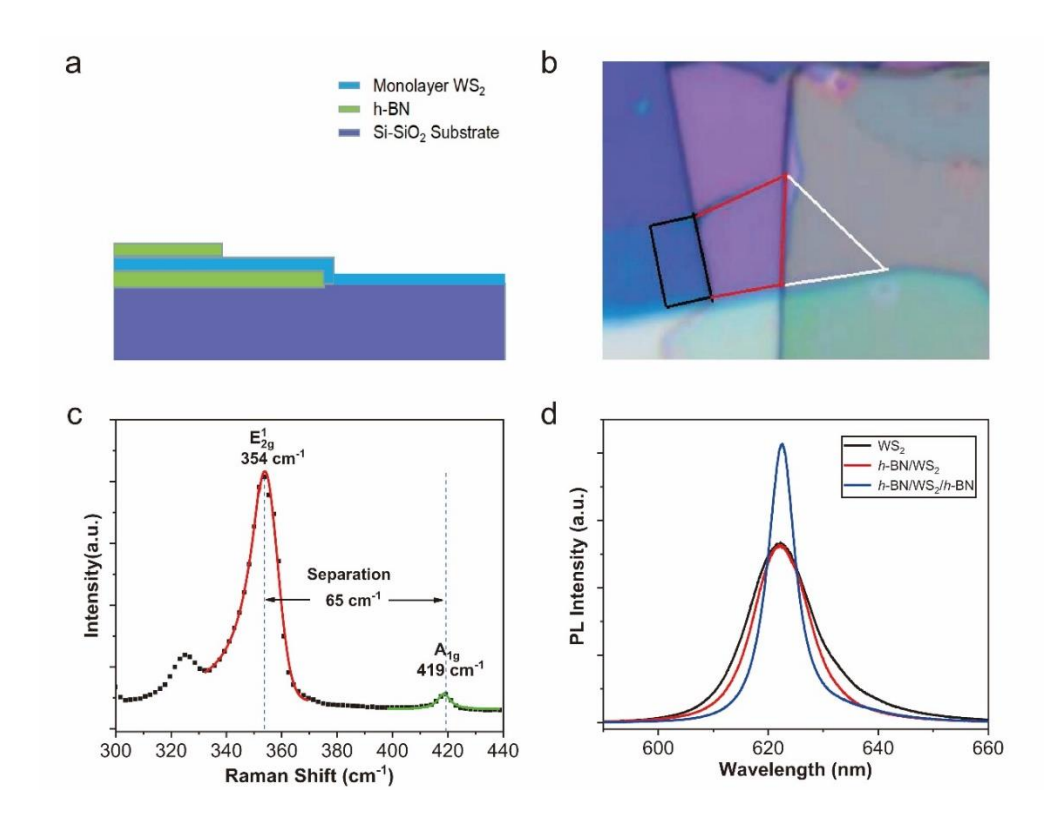


Figure 1
a) Schematics of the structure of the sample that contains regions of a WS₂ 1L under different dielectric environments. b) Optical microscope image of the sample. c) Raman spectrum of the WS₂ 1L on SiO₂. d) Photoluminescence spectra of the three regions of the sample under same conditions.

Figure 1d shows the photoluminescence (PL) spectra of the three regions of the sample obtained under the same conditions of 532-nm excitation with a power of 13 μW. Compared to WS₂/SiO₂ (black), the bottom *h*-BN makes the PL linewidth slightly narrower (red), while the PL yield is nearly unchanged. The *h*-BN/WS₂/*h*-BN region has the narrowest and highest peak (blue). The effect of *h*-BN on the linewidth can be attributed to the suppression of charge transfer from the substrate and air. Interestingly, the peak position is nearly identical in all three regions, which reflects the near-perfect

cancellation of the changes in the bandgap and exciton binding energy of WS₂ by *h*-BN. ^[47, 60-62] The small shift of the PL peak positions (within 1 nm) also confirms that the h-BN layers do not introduce a significant amount of strain to WS₂. It has been shown that the A-exciton PL peak of monolayer WS₂ shifts linearly with strain: A 1% of strain can shift the PL by about 5 nm. ^[63] Hence, the effect of strain on the excitonic dynamics in these samples is negligible.

2.2 Low-density excitonic dynamics

We first studied excitonic dynamics at low-density regimes, where exciton-exciton interaction can be ignored, by transient absorption measurements. In these experiments, a 200-fs pump pulse with a central wavelength of 410 nm was used to inject free carriers by interband absorption. Dynamics of the injected carriers was monitored by measuring the different reflection of a 620-nm probe pulse. Here, the differential reflection is defined as $\Delta R/R_0 = (R-R_0)/R_0$, where R and R_0 are the probe reflection with and without the presence of the pump, respectively (see Experimental Section). For each region, the injected carrier density is about 5×10^{11} cm⁻², which is estimated by using the pump fluence and the absorbance of the sample obtained by taking into account transmission and reflection of the multilayer structure^[64]. For each region, when the pump fluence was increased or decrease by a factor of two, no changes in the exciton dynamics were observed and the signal magnitude changes linearly with the fluence. This confirms the low-density regime of these measurements.

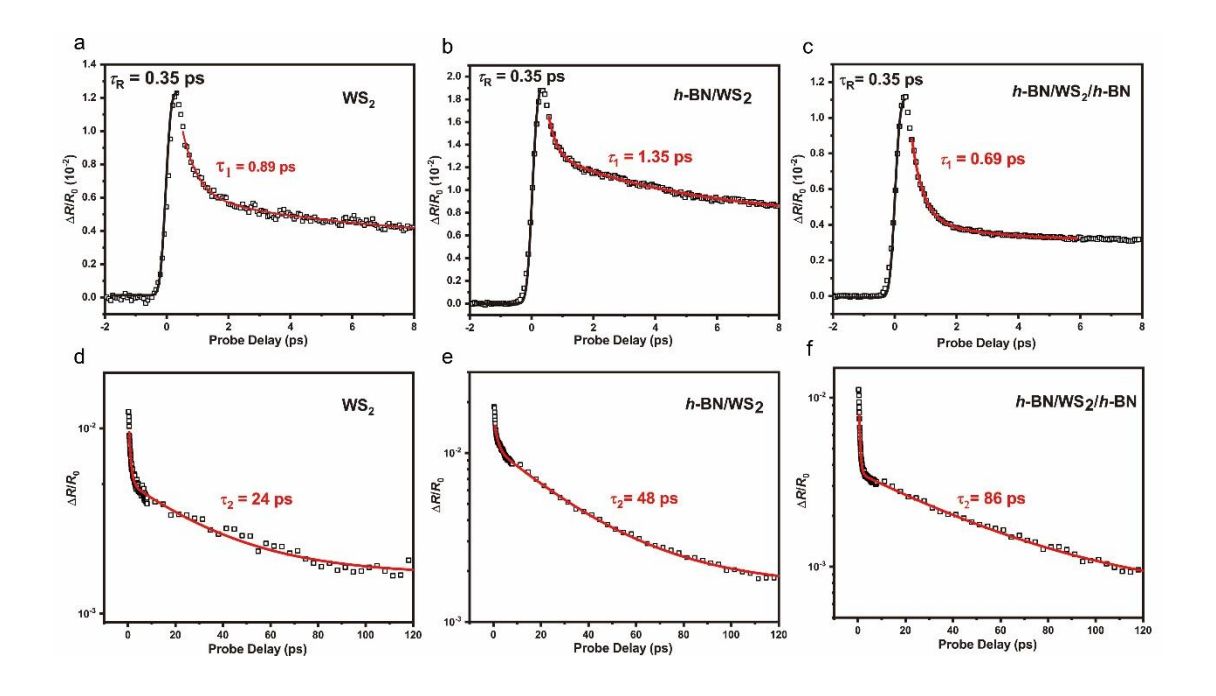


Figure 2
Differential reflection signal measured from the three regions of the sample over short (a-c) and long (d-f) time ranges.

Figure 2a, 2b, and 2c show the differential reflection signal over a short time range near the zero probe delay measured from the regions of WS₂, *h*-BN/WS₂, and *h*-BN/WS₂/*h*-BN, respectively. In each case, the signal reaches a peak on an ultrashort time scale. The rising part of the signal can be fit by a Gaussian integral with a full-width at half-maximum of about 0.35 ps. This is close to the time resolution of the experimental setup. With a high excitation excess energy, the pump pulse injects free carriers with high kinetic energies of several hundred meV. Thermalization and energy relaxation of these hot carriers increase the efficiency of these carriers of producing transient absorption of the probe, which is tuned to the A exciton. Hence, these processes should cause an increase of the differential reflection signal. The fact that the rising time is close to the time resolution of the experimental setup indicates that the

thermalization and energy relaxation processes in all regions occur on a time much shorter than 200 fs. Previously, thermalization and energy relaxation in thin MoS_2 has been found to occur on a time scale shorter than 100 fs. [17, 65] Our results are consistent with these studies. The ultrafast thermalization and energy relaxation in 2D materials can be attributed to the enhanced electron-electron and electron-phonon interactions due to the reduced dielectric screening. Our results indicate that the top h-BN layer does not cause a noticeable increase in the thermalization and energy relaxation times.

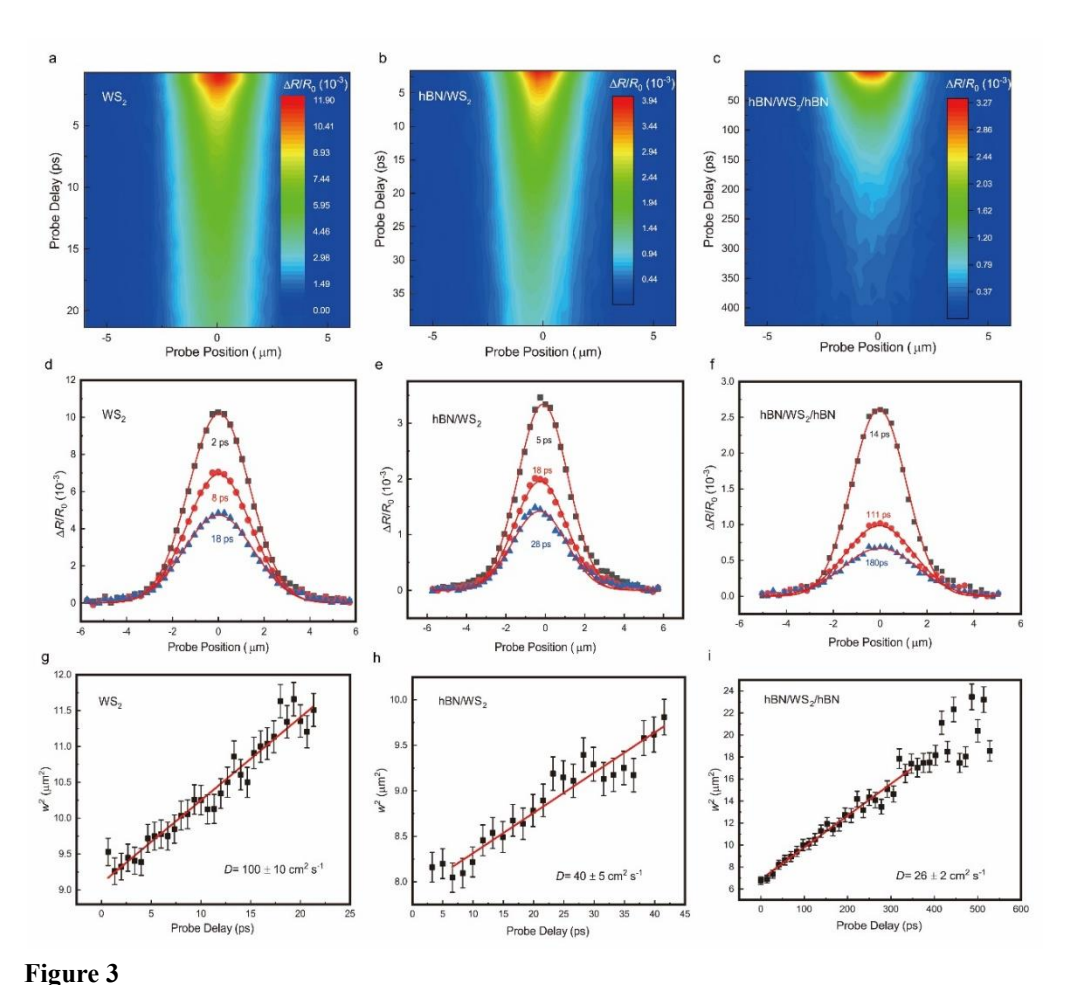
Figure 2d, 2e, and 2f show the differential reflection signal measured from these three regions over a longer time range. We found that in each region the decay of the signal after the peak is a bi-exponential process, as indicated by bi-exponential fits shown as the red curves in Figure 2. The short time constants on the order of 1 ps are labeled in 2a, 2b, and 2c. This fast decay process has been assigned to the formation of excitons from the injected free electron-hole pairs based on several experimental evidence. [18, 43] The exciton formation time of 0.89 ps in WS₂ is reasonably consistent with the previous measurements.^[18] By inserting the 95-nm h-BN layer between SiO₂ and WS₂, the exciton formation time is increased to 1.35 ps. It has been known that the doping effect of SiO₂^[28, 34] can significantly change the background carrier density of 2D TMDs. [66] The profound effect of inserted h-BN layers is to suppress charge transfer and the doping effect. [67] We can thus attribute the slower exciton formation with the h-BN layer to the lower background carrier density or change of interlayer phonon modes. In h-BN/WS₂/h-BN, the exciton formation time is 0.69 ps, significantly shorter than in h-BN/WS₂. Thus, the top h-BN facilitates exciton formation, which could be

due to the additional interfacial phonon modes that are available to participate in the exciton formation process. ^[68]

After the excitons are formed, the rest of the decay of the signal is controlled by exciton recombination. For WS₂, the decay constant is about 24 ps (Figure 2d). This lifetime is similar to previously reported values for WS₂ on SiO₂ ^[28,34] and is dominated by nonradiative recombination. ^[69] The exciton lifetime is increased to about 48 ps by inserting the *h*-BN layer between SiO₂ and WS₂ [Figure 2e]. In the region of *h*-BN/WS₂/*h*-BN, the exciton lifetime is further improved to 86 ps. We attribute the increase of the lifetime to suppression of nonradiative recombination of excitons on the surface and interface defects by the dangling-bond-free *h*-BN surface. These defects were known to facilitate Auger recombination of excitons in 2D TMDs. ^[70]

To study the effect of the *h*-BN layers on the transport properties of excitons, we measured the exciton diffusion coefficient in each region of the sample by performing spatially and temporally resolved transient absorption measurements. The tightly focused pump spot produces excitons with a Gaussian density profile. Due to the exciton diffusion, the density profile is expected to broaden. To monitor that, the probe spot was also tightly focused and spatially scanned, so that the differential reflection signal can be measured as a function of both the probe delay and the probe position (with respect to the center of the pump spot). Specifically, the probe spot was scanned by tilting a mirror in the probe arm, and at each probe position, the signal was measured as the probe delay was scanned. To ensure that the measurement was performed in the linear regime, the pump fluence used is sufficiently low in each measurement. Figure

3a - 3c shows the differential reflection signal measured by this method from the regions of WS₂, h-BN/WS₂, and h-BN/WS₂/h-BN, respectively. For each case, a few examples of the spatial profiles at varies probe delays are shown as the symbols in Figure 3d - 3f. By fitting these profiles (as well as those not shown) by Gaussian functions (curves), we obtained the squared width (w^2 , defined as the square of the full width at half maximum) as a function of the probe delay, as summarized in Figure 3g - 3i.



a) - c): Spatiotemporally resolved differential reflection signal measured from regions of WS₂ (a), h-BN/WS₂ (b), and h-BN/WS₂/h-BN (c), respectively. d - f): Examples of spatial profiles (symbols) and corresponding Gaussian fits (curves). g - i): Squared width of the profile deduced from the fits as a function of the probe delay (symbols). The red lines are linear fits.

The broadening of the exciton density profile observed in Figure 3 can be attributed to the exciton in-plane diffusion driven by the density gradient. By solving the diffusion-recombination equation, it is straightforward to show that the squared width of the profile increases linearly, with the rate related to the exciton diffusion coefficient,

$$w^2 = w_0^2 + 11.09Dt (1)$$

where w_0 is the initial width of the profile and D, the exciton diffusion coefficient. ^[71] With linear fits to the data shown in Figure 3g, 3h, and 3i, we obtained exciton diffusion coefficients of 100 ± 10 cm² s⁻¹ for WS₂, 40 ± 5 cm² s⁻¹ for h-BN/WS₂, and 26 ± 2 cm² s⁻¹ for the h-BN/WS₂/h-BN regions, respectively.

To understand the observed trend, we start by noting that the diffusion coefficient obtained from 1L WS₂ is reasonably consistent with previous results. Previously, we have obtained a diffusion coefficient of 60 ± 20 cm² s⁻¹ for 1L WS₂ on a Si/SiO₂ substrate at room temperature.^[34] Considering the development of 2D crystal synthesis techniques, a moderate improvement on the crystalline quality and thus the reduce defect scattering and increased exciton diffusion coefficient appear to be reasonable. In comparison, the exciton diffusion coefficient in h-BN/WS₂/h-BN, about 4 times smaller.

The observed suppression of the exciton diffusion by the h-BN layers is somewhat surprising. It has been generally recognized that by interfacing 2D materials with h-BN, the device performance is often improved. For example, previous studies have shown that h-BN and other dielectric layers can improve charge carrier mobility in 2D semiconductor devices, such as MoTe₂, [72] black phosphorus, [73-74] ReS₂, [75] and WS₂

field-effect transistors.^[76] However, our study has two distinct differences from these works. First, the quasiparticles studies here are excitons. As neutral particles, excitons suffer less scattering from charged impurities, which was the major limit on charge-carrier mobilities.^[72-74] Second, the measurements were performed from the same flake of 1L WS₂, and thus potential influences of sample quality variation and device qualities do not influence the results. We attribute the suppression of the exciton diffusion by the *h*-BN layers to additional photon scattering mechanisms introduced by *h*-BN. By interfacing with crystalline *h*-BN layers, excitons in WS₂ can scatter with phonons in *h*-BN and the new interfacial phonon modes. Since the exciton diffusion coefficient is mostly controlled by the exciton-phonon scattering, the additional scattering channels are expected to reduce the exciton mean free path, and thus the diffusion coefficient. However, to fully understand this trend at a quantitative level, more efforts, especially from the theoretical side, are necessary.

2.3. High-density excitonic dynamics

Exciton-exciton interaction is an important aspect of the exciton dynamics. Hence, it is interesting to study the effect of dielectric environment on exciton dynamics in high-density regimes. Since in such regimes the linear relation between the exciton density and the signal no longer holds, we first need to obtain this relation. The black symbols in Figure 3a - 3c show the peak differential reflection signal as a function of the injected carrier density for the three regions of the sample. For each region, the peak signal is proportional to the density in the low-density regime. However, with elevated densities,

deviation from the linear relation is clearly observed. Such a saturation of the transient absorption has been previously modeled by with a saturation density, N_s , through

$$\Delta R/R_0 = AN/(N+N_s) \tag{2}$$

where N is the carrier density and A, a dimensionless factor. ^[77] With this model, we can fit the results well (black curves in Figure 4). The saturation densities extracted from the three regions are similar. We consider the difference to be within our experimental error, because the carrier density in each case was deduced from the pump fluence by modeling multilayer reflection, which could introduce large uncertainties.

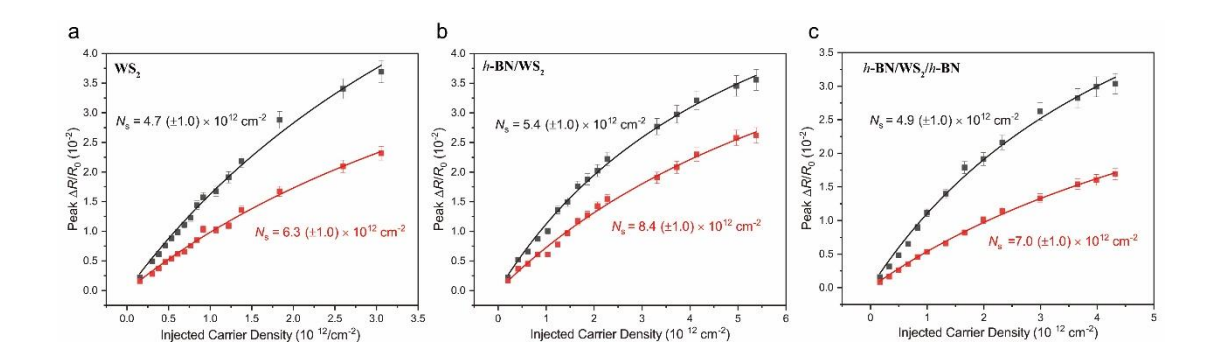


Figure 4Peak differential reflection signal of the 620-nm probe (black symbols) and the signal at a probe delay of 2 ps (red symbols) as a function of the carrier density injected by the pump. Panels a), b), and c) are results from the three regions of WS₂, *h*-BN/WS₂, and *h*-BN/WS₂/*h*-BN, respectively. The solid lines are fits (see text).

Interestingly, when the signal at a probe delay of 2 ps was analyzed (red symbols and curves in Figure 4), larger saturation densities are obtained in all the regions. As discussed above, the injected carriers form excitons on a picosecond time scale. Hence, the saturation densities obtained from fitting the peak signal describes the saturation effect of free carriers, while that at 2 ps, the effect of excitons. Therefore, the saturation density of excitons is higher than free electron-hole pairs. This effect could be attributed

to the smaller size of excitons compared to electron-hole pairs. ^[78] A quantitative description of this effect is beyond the scope of this work; however, the results could help develop a theoretical understanding of the saturation effect of excitons and free carriers.

We next studied the effect of dielectric environment on exciton-exciton annihilation. Previous studies have shown that in TMD 1Ls on Si/SiO₂, exciton-exciton annihilation is a dominating process in excitonic dynamics at high densities above 10¹³ cm⁻². [19-20, 35, 79-84] In 2D materials, exciton-exciton annihilation was significantly more efficient than 3D semiconductors, posing a limiting factor on the performance of devices with high injection levels. Hence, it is interesting to study the effect of dielectric environment on this process. Figure 5a shows the differential reflection signal measured from the *h*-BN/WS₂/*h*-BN region with different levels of injected carrier density, as labeled in the panels. By using the relation established in Figure 3c, red curve, the signal is converted to the exciton density (Figure 5b). With the exciton-exciton annihilation, the exciton density evolves as

$$dN/dt = -N/\tau_2 - \gamma N^2 / 2 \tag{3}$$

where τ_2 and γ are the exciton lifetime and exciton-exciton annihilation rate, respectively^[85]. In the time range much shorter than the lifetime, the recombination contribution can be ignored, leading to a simple solution of

$$N_0/N - 1 = \gamma N_0 t \tag{4}$$

where N_0 is the initially injected density. To compare with this model, we calculate N_0/N - 1 from N shown in Figure 5b, and plot it as a function of probe delay in Figure 5c.

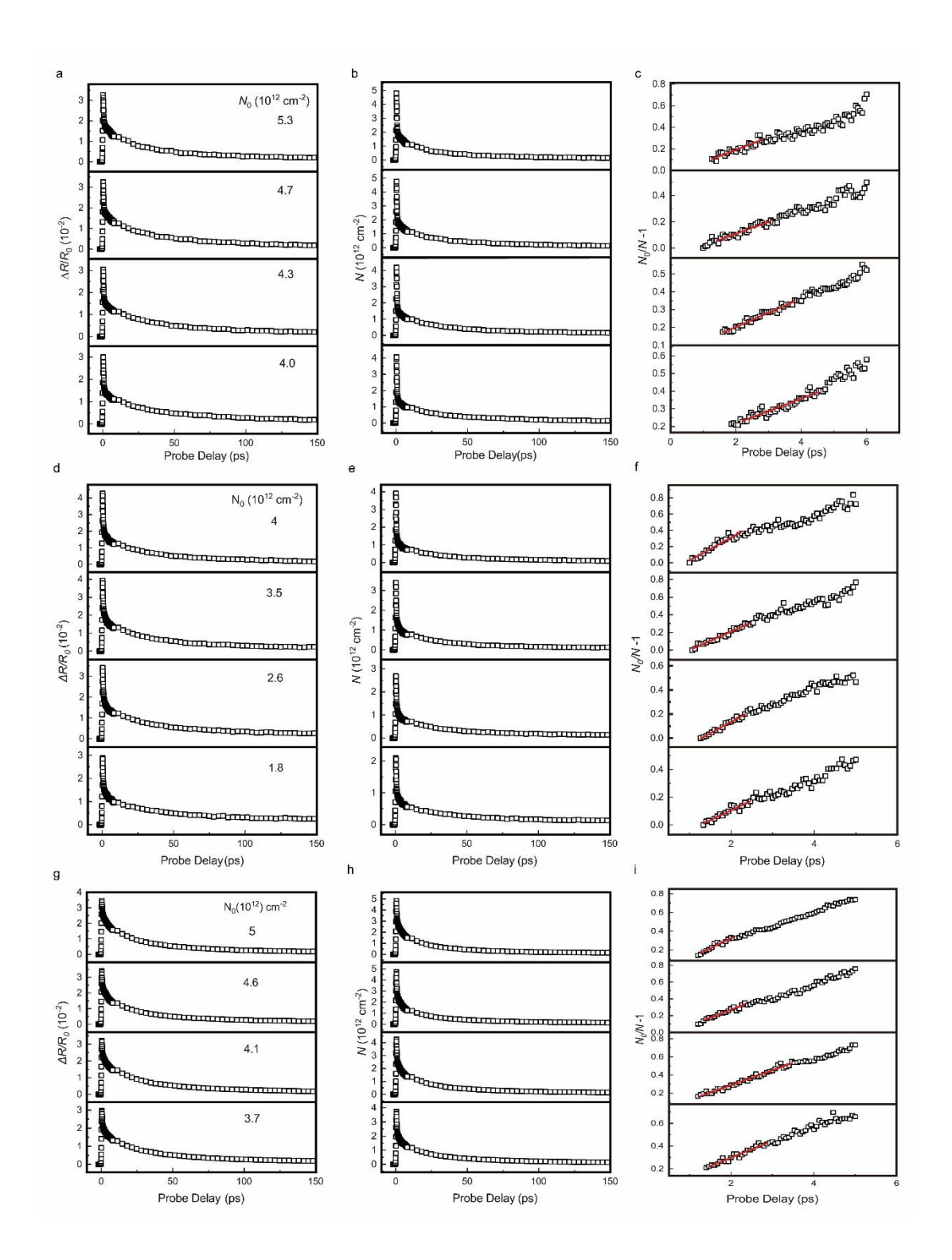


Figure 5 a) Differential reflection signal measured in the region of h-BN/WS₂/h-BN with different levels of injected carrier density. b) Deduced exciton density as a function of probe delay by using the saturation model. c) The quantity $N_0/N - 1$ as a function of probe delay. d), e), f) same as a), b), c) but for the region of WS₂. g), h), i) same as a), b), c) but for the region of h-BN/WS₂.

The linear relation in the first a few picosecond shows that the model can adequately describe the observation. Similar measurements were performed in the other two regions of the sample, too. The results show in Figure 5d, e, f, g, h, and i.

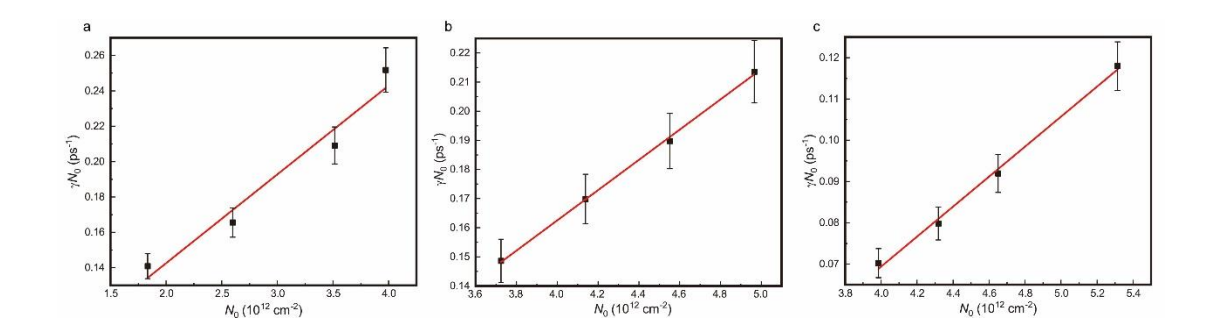


Figure 6 The slope, γN_0 , as a function of N_0 obtained from regions of WS₂ a), h-BN/WS₂ b), and h-BN/WS₂/h-BN c).

To obtain the exciton-exciton annihilation rate, we plot in Figure 6 the slopes deduced from linear fits shown in Figure 5c, f, and i. Clearly, the slope γN_0 is proportional to N_0 , as expected. Linear fits (red lines) give the exciton-exciton annihilation rates of 0.050 ± 0.004 , 0.052 ± 0.004 , and 0.036 ± 0.004 cm²/s for the regions of WS₂, h-BN/WS₂, and h-BN/WS₂/h-BN, respectively. Hence, the top h-BN only reduces the annihilation rate by a small amount. It is somewhat surprising that the dielectric environment only has a small effect on the exciton-exciton annihilation. We attribute this observation to the fact that excitons are neutral quasiparticles, and hence their interactions are less sensitive to the screening of the Coulomb field between charge carriers.

3 Conclusion

In summary, excitonic dynamics in WS2 1L under different dielectric environments was studied by transient absorption measurements. Different regions of a single WS₂ 1L are subject to different environments of air/SiO₂, air/h-BN, and h-BN/h-BN, respectively. Upon ultrafast excitation of free electron-hole pairs by a femtosecond laser pulse, the thermalization and relaxation of the hot carriers are found to be much faster than the time resolution of the study of about 350 fs, showing the efficient thermalization and relaxation even with h-BN dielectric screening. We found that the top h-BN layer reduced the exciton formation time by about 50%, which can be attributed to the additional interlayer phonon modes available to assist the exciton formation process. Both the bottom and the top h-BN layers were found to be effective in prolonging the exciton lifetime. The h-BN sandwiched sample shows an exciton lifetime of more than 80 ps, which is 3 - 4 times longer than WS₂ on SiO₂. We found that the h-BN cap and underlay layers suppress the exciton diffusion in monolayer WS₂. Compared to a SiO₂ substrate, the exciton diffusion coefficient in WS₂ on h-BN shows a reduction of about a factor of 2.5, from about 100 to about 40 cm² s⁻¹. An h-BN cap layer further reduced the diffusion coefficient to about 26 cm² s⁻¹. The suppression of the exciton diffusion by the h-BN layers was attributed to additional phonon scattering mechanisms introduced by h-BN, which decreases the exciton mean free path. Furthermore, the effects of the h-BN layers on high-density excitonic dynamics were also studied. These experimental results provide useful information for designing and understanding the effect of h-BN layers in 2D devices, especially optoelectronic

devices where excitons play important roles.

4 Experimental section

In our sample fabrication process, first, two thick h-BN flakes and one WS₂ 1L mechanically exfoliated from bulk crystals three different onto polydimethylsiloxane (PDMS) substrates using scotch tapes. One of the h-BN flakes was then transferred onto a Si substrate covered with a 300-nm SiO₂ layer. Next, the WS₂ 1L was transferred to the substrate such that one part of it was on top of h-BN with the rest directly on SiO₂. Finally, the other h-BN was transferred so that it covers part of the WS₂ flake that is on h-BN. After the transfer of each layer, the sample was annealed under the H₂-Ar gas environment at 200°C for 6 hours to improve the quality of the interfaces.

The excitonic dynamics was studied by transient absorption measurements in reflection geometry. A Ti-doped sapphire oscillator generates 100-fs pulses at 820 nm with a repetition rate of 80 MHz. The output is divided into two parts. One part pumps a visible optical parametric oscillator to generate a tunable output around 620 nm, which was used in the measurement as the probe. The other part is focused on a beta barium borate crystal to generate its second harmonic at 410 nm, serving as the pump. The propagation length of the pump pulse is controlled by a retroreflector that is installed on a motorized stage. The pump and probe beams are combined by a beamsplitter and focused on the sample by a microscope objective lens. The probe reflection is collimated by the objective lens and is sent to a silicon photodiode. The

voltage of the photodiode is measured by a lock-in amplifier that is synchronized with a mechanical chopper that modulates the pump intensity at about 2 kHz. To reveal the spatiotemporal dynamics of the excitons, the differential reflection signal was measured as a function of space and time. The time resolution was obtained by changing the distance the probe beam travels by using a mirror mounted on a linear stage. The spatial resolution was achieved by scanning the probe spot across the pump spot by tilting a mirror in the probe arm with a motorized mirror mount. All measurements were performed with the sample at room temperature and exposed to air.

Acknowledgment

The authors thank the financial support of the National Key R&D Program of China (2016YFA0202302), the National Natural Science Foundation of China (61527817 and 61875236), Overseas Expertise Introduction Center for Discipline Innovation, 111 Center of China, and National Science Foundation of USA (DMR-1505852).

References

- [1] Z. Lin, A. McCreary, N. Briggs, S. Subramanian, K. H. Zhang, Y. F. Sun, X. F. Li, N. J. Borys, H. T. Yuan, S. K. Fullerton-Shirey, A. Chernikov, H. Zhao, S. McDonnell, A. M. Lindenberg, K. Xiao, B. J. LeRoy, M. Drndic, J. C. M. Hwang, J. Park, M. Chhowalla, R. E. Schaak, A. Javey, M. C. Hersam, J. Robinson, M. Terrones, *2D Mater.* **2016**, *3*, 042001.
- [2] K. F. Mak, C. Lee, J. Hone, J. Shan, T. F. Heinz, Phys. Rev. Lett. 2010, 105, 136805.
- [3] A. Splendiani, L. Sun, Y. Zhang, T. Li, J. Kim, C.-Y. Chim, G. Galli, F. Wang, *Nano Lett.* **2010**, *10*, 1271-1275.
- [4] H. Zeng, G.-B. Liu, J. Dai, Y. Yan, B. Zhu, R. He, L. Xie, S. Xu, X. Chen, W. Yao, X. Cui, *Sci. Rep.* **2013**, *3*, 1608.
- [5] N. Kumar, S. Najmaei, Q. Cui, F. Ceballos, P. M. Ajayan, J. Lou, H. Zhao, *Phys. Rev. B* **2013**, *87*, 161403.
- [6] L. M. Malard, T. V. Alencar, A. P. M. Barboza, K. F. Mak, A. M. de Paula, Phys. Rev. B 2013, 87,

- 201401.
- [7] Y. Li, Y. Rao, K. F. Mak, Y. You, S. Wang, C. R. Dean, T. F. Heinz, Nano Lett. 2013, 13, 3329-3333.
- [8] X. Yin, Z. Ye, D. A. Chenet, Y. Ye, K. O'Brien, J. C. Hone, X. Zhang, Science 2014, 344, 488-490.
- [9] B. W. H. Baugher, H. O. H. Churchill, Y. Yang, P. Jarillo-Herrero, *Nat. Nanotechnol.* **2014**, *9*, 262-267.
- [10] Y. J. Zhang, T. Oka, R. Suzuki, J. T. Ye, Y. Iwasa, Science 2014, 344, 725-728.
- [11] J. S. Ross, P. Klement, A. M. Jones, N. J. Ghimire, J. Yan, D. G. Mandrus, T. Taniguchi, K. Watanabe, K. Kitamura, W. Yao, D. H. Cobden, X. Xu, *Nat. Nanotechnol.* **2014**, *9*, 268-274.
- [12] A. Pospischil, M. M. Furchi, T. Mueller, Nat. Nanotechnol. 2014, 9, 257-261.
- [13] K. F. Mak, K. He, C. Lee, G. H. Lee, J. Hone, T. F. Heinz, J. Shan, Nat. Mater. 2013, 12, 207-211.
- [14] J. S. Ross, S. Wu, H. Yu, N. J. Ghimire, A. M. Jones, G. Aivazian, J. Yan, D. G. Mandrus, D. Xiao, W. Yao, X. Xu, *Nat. Commun.* **2013**, *4*, 1474.
- [15] A. Chernikov, T. C. Berkelbach, H. M. Hill, A. Rigosi, Y. L. Li, O. B. Aslan, D. R. Reichman, M. S. Hybertsen, T. F. Heinz, *Phys. Rev. Lett.* **2014**, *113*, 076802.
- [16] K. He, N. Kumar, L. Zhao, Z. Wang, K. F. Mak, H. Zhao, J. Shan, Phys. Rev. Lett. 2014, 113, 026803.
- [17] Z. Nie, R. Long, L. Sun, C. C. Huang, J. Zhang, Q. Xiong, D. W. Hewak, Z. Shen, O. V. Prezhdo, Z. H. Loh, *ACS Nano* **2014**, *8*, 10931-10940.
- [18] F. Ceballos, Q. Cui, M. Z. Bellus, H. Zhao, Nanoscale 2016, 8, 11681-11688.
- [19] N. Kumar, Q. Cui, F. Ceballos, D. He, Y. Wang, H. Zhao, Phys. Rev. B 2014, 89, 125427.
- [20] D. Sun, Y. Rao, G. A. Reider, G. Chen, Y. You, L. Brezin, A. R. Harutyunyan, T. F. Heinz, *Nano Lett.* **2014**, *14*, 5625-5629.
- [21] B. A. Ruzicka, S. Wang, L. K. Werake, B. Weintrub, K. P. Loh, H. Zhao, *Phys. Rev. B* **2010**, *82*, 195414.
- [22] J. He, D. He, Y. Wang, Q. Cui, M. Z. Bellus, H.-Y. Chiu, H. Zhao, ACS Nano 2015, 9, 6436-6442.
- [23] R. Wang, B. A. Ruzicka, N. Kumar, M. Z. Bellus, H.-Y. Chiu, H. Zhao, *Phys. Rev. B* **2012**, *86*, 045406.
- [24] Q. Wang, S. Ge, X. Li, J. Qiu, Y. Ji, J. Feng, D. Sun, ACS Nano 2013, 7, 11087-11093.
- [25] C. Mai, A. Barrette, Y. Yu, Y. G. Semenov, K. W. Kim, L. Cao, K. Gundogdu, *Nano Lett.* **2013**, *14*, 202-206.
- [26] S. Dal Conte, F. Bottegoni, E. A. A. Pogna, D. De Fazio, S. Ambrogio, I. Bargigia, C. D'Andrea, A. Lombardo, M. Bruna, F. Ciccacci, A. C. Ferrari, G. Cerullo, M. Finazzi, *Phys. Rev. B* **2015**, *92*, 235425.
- [27] N. Kumar, J. He, D. He, Y. Wang, H. Zhao, Nanoscale **2014**, *6*, 12690-12695.
- [28] C. Mai, Y. G. Semenov, A. Barrette, Y. F. Yu, Z. H. Jin, L. Y. Cao, K. W. Kim, K. Gundogdu, *Phys. Rev. B* **2014**, *90*, 041414.
- [29] C. R. Zhu, K. Zhang, M. Glazov, B. Urbaszek, T. Amand, Z. W. Ji, B. L. Liu, X. Marie, *Phys. Rev. B* **2014**, *90*, 161302.
- [30] W. T. Hsu, Y. L. Chen, C. H. Chen, P. S. Liu, T. H. Hou, L. J. Li, W. H. Chang, *Nat. Commun.* **2015**, *6*, 8963.
- [31] L. Y. Yang, N. A. Sinitsyn, W. B. Chen, J. T. Yuan, J. Zhang, J. Lou, S. A. Crooker, *Nat. Phys.* **2015**, *11*, 830-834.
- [32] L. Y. Yang, W. B. Chen, K. M. McCreary, B. T. Jonker, J. Lou, S. A. Crooker, *Nano Lett.* **2015**, *15*, 8250-8254.
- [33] H. Shi, R. Yan, S. Bertolazzi, J. Brivio, B. Gao, A. Kis, D. Jena, H. G. Xing, L. Huang, *ACS Nano* **2012**, 7, 1072-1080.
- [34] J. He, D. He, Y. Wang, Q. Cui, F. Ceballos, H. Zhao, Nanoscale 2015, 7, 9526.

- [35] L. Yuan, L. B. Huang, Nanoscale 2015, 7, 7402-7408.
- [36] Q. Cui, F. Ceballos, N. Kumar, H. Zhao, ACS Nano 2014, 8, 2970-2976.
- [37] C. J. Docherty, P. Parkinson, H. J. Joyce, M. H. Chiu, C. H. Chen, M. Y. Lee, L. J. Li, L. M. Herz, M. B. Johnston, *ACS Nano* **2014**, *8*, 11147-11153.
- [38] T. Yan, X. Qiao, X. Liu, P. Tan, X. Zhang, Appl. Phys. Lett. 2014, 105, 101901.
- [39] H. N. Wang, C. J. Zhang, F. Rana, Nano Lett. 2015, 15, 8204-8210.
- [40] M. Seo, H. Yamaguchi, A. D. Mohite, S. Boubanga-Tombet, J. C. Blancon, S. Najmaei, P. M. Ajayan, J. Lou, A. J. Taylor, R. P. Prasankumar, *Sci. Rep.* **2016**, *6*, 21601.
- [41] Y. M. You, X. X. Zhang, T. C. Berkelbach, M. S. Hybertsen, D. R. Reichman, T. F. Heinz, *Nat. Phys.* **2015**, *11*, 477-481.
- [42] K. Hao, J. F. Specht, P. Nagler, L. Xu, K. Tran, A. Singh, C. K. Dass, C. Schüller, T. Korn, M. Richter, A. Knorr, X. Li, G. Moody, *Nat. Commun.* **2017**, *8*, 15552.
- [43] P. Steinleitner, P. Merkl, P. Nagler, J. Mornhinweg, C. Schuller, T. Korn, A. Chernikov, R. Huber, *Nano Lett.* **2017**, *17*, 1455-1460.
- [44] Y. Lin, X. Ling, L. Yu, S. Huang, A. L. Hsu, Y. H. Lee, J. Kong, M. S. Dresselhaus, T. Palacios, *Nano Lett* **2014**, *14* (10), 5569-76.
- [45] A. V. Stier, N. P. Wilson, G. Clark, X. Xu, S. A. Crooker, Nano Lett. 2016, 16 (11), 7054-7060.
- [46] J. He, N. Kumar, M. Z. Bellus, H.-Y. Chiu, D. He, Y. Wang, H. Zhao, Nat. Commun. 2014, 5, 5622.
- [47] A. Raja, A. Chaves, J. Yu, G. Arefe, H. M. Hill, A. F. Rigosi, T. C. Berkelbach, P. Nagler, C. Schuller, T. Korn, C. Nuckolls, J. Hone, L. E. Brus, T. F. Heinz, D. R. Reichman, A. Chernikov, *Nat. Commun.* **2017**, *8*, 15251.
- [48] S. M. Cui, H. H. Pu, S. A. Wells, Z. H. Wen, S. Mao, J. B. Chang, M. C. Hersam, J. H. Chen, *Nat. Commun.* **2015**, *6*, 8632.
- [49] Z. B. Song, T. Schultz, Z. J. Ding, B. Lei, C. Han, P. Amsalem, T. T. Lin, D. Z. Chi, S. L. Wong, Y. J. Zheng, M. Y. Li, L. J. Li, W. Chen, N. Koch, Y. L. Huang, A. T. S. Wee, *ACS Nano* **2017**, *11*, 9128-9135.
- [50] J. H. Kim, J. Lee, J. H. Kim, C. C. Hwang, C. Lee, J. Y. Park, Appl. Phys. Lett. 2015, 106, 251606.
- [51] Y. Li, C. Y. Xu, L. Zhen, Appl. Phys. Lett. 2013, 102, 143110.
- [52] P. Bolshakov, P. Zhao, A. Azcatl, P. K. Hurley, R. M. Wallace, C. D. Young, *Appl. Phys. Lett.* **2017**, *111*, 032110.
- [53] O. Ajayi, J. V. Ardelean, G. D. Shepard, J. Wang, A. Antony, T. Taniguchi, K. Watanabe, T. Heinz, S. Strauf, X. Y. Zhu, J. C. Hone, *2D Mater.* **2017**, *4*.
- [54] S. Lippert, L. Schneider, D. Renaud, K. Kang, O. Ajayi, M.-U. Halbich, O. Abdulmunem, X. Lin, J. Kuhnert, K. Hassoon, S. Edalati Boostan, Y. Kim, W. Heimbrodt, E.-H. Yang, J. Hone, A. Rahimi-Iman, *2D Mater.* **2016**, *4*, 025045.
- [55] Y. Yu, Y. Yu, C. Xu, Y.-Q. Cai, L. Su, Y. Zhang, Y.-W. Zhang, K. Gundogdu, L. Cao, *Adv. Funct. Mater.* **2016**, *26*, 4733-4739.
- [56] Y. Hoshi, T. Kuroda, M. Okada, R. Moriya, S. Masubuchi, K. Watanabe, T. Taniguchi, R. Kitaura, T. Machida, *Phys. Rev. B* **2017**, *95*.
- [57] L. M. Schneider, S. Lippert, J. Kuhnert, O. Ajayi, D. Renaud, S. Firoozabadi, Q. Ngo, R. Guo, Y. D. Kim, W. Heimbrodt, J. C. Hone, A. Rahimi-Iman, *Nano-Structures & Nano-Objects* **2018**, *15*, 84 97. [58] F. Ceballos, P. Zereshki, H. Zhao, *Phys.rev.materials* **2017**, *1* (4).
- [59] J. T. Mlack, P. Masih Das, G. Danda, Y.-C. Chou, C. H. Naylor, Z. Lin, N. P. López, T. Zhang, M. Terrones, A. T. C. Johnson, *Sci. Rep.* **2017**, *7*, 43037.
- [60] G. Gupta, S. Kallatt, K. Majumdar, Phys. Rev. B 2017, 96, 081403.

- [61] K. T. Winther, K. S. Thygesen, 2D Mater. 2017, 4, 025059.
- [62] Y. S. Cho, T. C. Berkelbach, Phys. Rev. B 2018, 97, 041409.
- [63] Y. Wang, C. Cong, W. Yang, J. Shang, N. Peimyoo, Y. Chen, J. Kang, J. Wang, W. Huang, T. Yu, *Nano Res.* **2015**, *8* (8), 2562-2572.
- [64] F. Ceballos, P. Zereshki, H. Zhao, Phys. Rev. Mater. 2017, 1, 044001.
- [65] A. Steinhoff, M. Florian, M. Rosner, M. Lorke, T. O. Wehling, C. Gies, F. Jahnke, *2D Mater.* **2016**, *3*, 031006.
- [66] K. Dolui, I. Rungger, S. Sanvito, Phys. Rev. B 2013, 87, 165402.
- [67] R. A. Doganov, S. P. Koenig, Y. T. Yeo, K. Watanabe, T. Taniguchi, B. Ozyilmaz, *Appl. Phys. Lett.* **2015**, *106*, 083505.
- [68] A. Thilagam, J. Appl. Phys. 2016, 120, 124306.
- [69] C. Robert, D. Lagarde, F. Cadiz, G. Wang, B. Lassagne, T. Amand, A. Balocchi, P. Renucci, S. Tongay, B. Urbaszek, X. Marie, *Phys. Rev. B* **2016**, *93*, 205423.
- [70] A. Alharbi, P. Zahl, D. Shahrjerdi, Appl. Phys. Lett. 2017, 110, 033503.
- [71] N. Kumar, J. He, D. He, Y. Wang, Z. Hui, J. Appl. Phys. 2013, 113 (13), 133702.
- [72] H. Ji, M. K. Joo, Y. Yun, J. H. Park, G. M. Lee, B. H. Moon, H. Yi, D. Suh, S. C. Lim, *ACS Appl. Mater. Interfaces* **2016**, *8* (29), acsami.6b02085.
- [73] G. Long, D. Maryenko, J. Shen, S. Xu, J. Hou, Z. Wu, W. K. Wong, T. Han, J. Lin, Y. Cai, *Nano Lett.* **2016**, *16* (12), 7768-7773.
- [74] R. A. Doganov, S. P. Koenig, Y. Yeo, K. Watanabe, T. Taniguchi, B. Özyilmaz, *Appl. Phys. Lett.* **2015**, *106* (8), 768.
- [75] G. Nazir, M. Abdul Rehman, M. Khan, G. Dastgeer, S. Aftab, A. Muhammad Afzal, Y. Seo, J. Eom, *ACS Appl. Mater.* **2018**.
- [76] F. Withers, T. H. Bointon, D. C. Hudson, M. F. Craciun, S. Russo, Sci. Rep. 2014, 4 (4), 4967.
- [77] F. Ceballos, H. Zhao, Adv. Funct. Mater. 2017, 27, 1604509.
- [78] S. Schmitt-Rink, D. S. Chemla, D. A. B. Miller, *Phys. Rev. B* **1985**, *32*, 6601-6609.
- [79] C. Poellmann, P. Steinleitner, U. Leierseder, P. Nagler, G. Plechinger, M. Porer, R. Bratschitsch, C. Schuller, T. Korn, R. Huber, *Nat. Mater.* **2015**, *14*, 889-893.
- [80] S. Kar, Y. Su, R. R. Nair, A. K. Sood, ACS Nano 2015, 9, 12004-12010.
- [81] H. N. Wang, J. H. Strait, C. J. Zhang, W. M. Chan, C. Manolatou, S. Tiwari, F. Rana, *Phys. Rev. B* **2015**, *91*, 165411.
- [82] S. Q. Zhao, D. W. He, J. Q. He, X. W. Zhang, L. X. Yi, Y. S. Wang, H. Zhao, *Nanoscale* **2018**, *10*, 9538-9546.
- [83] B. Liu, Y. Z. Meng, X. Z. Ruan, F. Q. Wang, W. Q. Liu, F. Q. Song, X. F. Wang, J. Wu, L. He, R. Zhang, Y. B. Xu, *Nanoscale* **2017**, *9*, 18546-18551.
- [84] V. Vega-Mayoral, D. Vella, T. Borzda, M. Prijatelj, I. Tempra, E. A. A. Pogna, S. D. Conte, P. Topolovsek, N. Vujicic, G. Cerullo, D. Mihailovic, C. Gadermaier, *Nanoscale* **2016**, *8*, 5428-5434.
- [85] Y. Z. Ma, L. Valkunas, S. L. Dexheimer, S. M. Bachilo, G. R. Fleming, *Phys. Rev. Lett.* **2005**, *94*, 157402.